



Cite this: *J. Mater. Chem. A*, 2015, 3, 22794

A high-performance hydroxyl-functionalized polymer of intrinsic microporosity for an environmentally attractive membrane-based approach to decontamination of sour natural gas†

Shouliang Yi,^a Xiaohua Ma,^b Ingo Pinnau^{*b} and William J. Koros^{*a}

Acid gases carbon dioxide (CO₂) and hydrogen sulfide (H₂S) are important and highly undesirable contaminants in natural gas, and membrane-based removal of these contaminants is environmentally attractive. Although removal of CO₂ from natural gas using membranes is well established in industry, there is limited research on H₂S removal, mainly due to its toxic nature. In actual field operations, wellhead pressures can exceed 50 bar with H₂S concentrations up to 20%. Membrane plasticization and competitive mixed-gas sorption, which can both lead to a loss of separation efficiency, are likely to occur under these aggressive feed conditions, and this is almost always accompanied by a significant decrease in membrane selectivity. In this paper, permeation and separation properties of a hydroxyl-functionalized polymer with intrinsic microporosity (PIM-6FDA-OH) are reported for mixed-gas feeds containing CO₂, H₂S or the combined pair with CH₄. The pure-gas permeation results show no H₂S-induced plasticization of the PIM-6FDA-OH film in a pure H₂S feed at 35 °C up to 4.5 bar, and revealed only a slight plasticization up to 8 bar of pure H₂S. The hydroxyl-functionalized PIM membrane exhibited a significant pure-gas CO₂ plasticization resistance up to 28 bar feed pressure. Mixed-gas (15% H₂S/15% CO₂/70% CH₄) permeation results showed that the hydroxyl-functionalized PIM membrane maintained excellent separation performance even under exceedingly challenging feed conditions. The CO₂ and H₂S permeability isotherms indicated minimal CO₂-induced plasticization; however, H₂S-induced plasticization effects were evident at the highest mixed gas feed pressure of 48 bar. Under this extremely aggressive mixed gas feed, the binary CO₂/CH₄ and H₂S/CH₄ permselectivities, and the combined CO₂ and H₂S acid gas selectivity were 25, 30 and 55, respectively. Our results indicate that OH-functionalized PIM materials are very promising candidate membrane materials for simultaneous removal of CO₂ and H₂S from aggressive natural gas feeds, which makes membrane-based gas separation technology an attractive option for clean energy production and reducing greenhouse gas emissions.

Received 31st July 2015
Accepted 24th September 2015

DOI: 10.1039/c5ta05928c

www.rsc.org/MaterialsA

Introduction

With the continuing growth in global population and development, the total worldwide demand for energy is projected to rapidly expand in the near future. In the Annual Energy Outlook (AEO) 2014 Reference case, total delivered energy consumption in the industrial sector is projected to increase by 28% from 2012 to 2040.¹ Much of the growth will reflect natural gas use, which is projected to account for 34% of the total

increase in energy consumption from 2012 to 2025 and 59% of the increase from 2025 to 2040. One of the reasons for this trend is that natural gas has relatively low carbon footprint, increased thermal efficiency, and cleaner burning benefits compared to other fossil fuels. These advantages make natural gas one of the cleanest and most efficient energy sources. Despite this promising outlook, raw natural gas can contain significant amounts of impurities such as hydrogen sulfide (H₂S), carbon dioxide (CO₂), water vapor, higher hydrocarbons, nitrogen, and other inert gases, which must be removed before pipeline delivery to industrial or household users. Among these impurities, the acid gas components CO₂ and H₂S are particularly important to be removed. Typical pipeline specifications in the US mandate a H₂S concentration below 4 ppm and CO₂ concentration below 2%.² Over 30% of the gas produced in the United States and over 40% of proven raw natural gas reserves

^aSchool of Chemical and Biomolecular Engineering, Georgia Institute of Technology, 311Ferst Drive, Atlanta, GA 30332, USA. E-mail: bill.koros@chbe.gatech.edu

^bAdvanced Membranes and Porous Materials Center, Physical Sciences and Engineering Division, King Abdullah University of Science and Technology, Thuwal 23955-6900, Saudi Arabia. E-mail: ingo.pinnau@kaust.edu.sa

† Electronic supplementary information (ESI) available: Pure and mixed gas permeation modelling. See DOI: 10.1039/c5ta05928c



contain CO₂ and H₂S above acceptable levels, and these wells are classified as sour gas.³ Recently, H₂S removal has received more attention, because in certain areas in the US, Canada, Russia, and the Middle East, oil and gas reservoirs were reported to contain H₂S as well as CO₂ at varying high levels.^{4–6} Currently, amine absorption dominates acid gas (CO₂ and H₂S) separation technology to reduce CO₂ and H₂S to meet the pipeline requirement (<2% CO₂, <4 ppm H₂S). Such processes present environmental concerns as well as high capital and maintenance costs of the large absorption units.⁷ On the other hand, compared to conventional absorption processes, membrane-based gas separation offers a potentially more energy efficient technology with low capital cost, small footprint, simple operation, and low maintenance, as well as minimal environmental impact.^{2,7} Membrane technology may also provide options for the bulk removal of CO₂ and H₂S, as well as other impurities through hybrid absorption-membrane processes.⁷ Despite these advantages, membrane-based processes require the development of improved membrane materials with both high productivity and high selectivity to minimize capital and operating cost.^{2,8–10} Moreover, for systems of highly interacting species such as CO₂ and H₂S, the stability of a membrane material to resist penetrant-induced plasticization presents an additional challenge.

Commercially available polymers for gas separation membranes (polysulfone, cellulose acetate, polyimide, *etc.*) are limited by their moderate permeability and selectivity.^{4,11–13} The most promising materials, glassy polyimides, especially 6FDA-based polyimides offer: (i) solubility in common processing solvents, (ii) thermal and chemical stability, and (iii) robust mechanical properties under high-pressure natural gas feeds.¹⁰ Moreover, some polyimides also offer excellent intrinsic CO₂/CH₄ separation properties, *i.e.*, high productivity and selectivity for feeds with low CO₂ partial pressures, and are processable into thin-skinned hollow-fibers by standard commercial fabrication processes.^{3,8,10,14–29} While many membrane materials have been developed for the separation of CO₂/CH₄ over the past several decades, only a few studies have focused on the development of materials for removal of all natural sour gas components due to the high toxicity of H₂S.^{3,4,11,21,22,24} To safely handle H₂S, additional strict safety measures are required, so the few literature studies addressing H₂S removal using membranes have generally focused on relatively low H₂S concentration and feed pressure.^{11,30} Such studies show that polymers with high H₂S/CH₄ selectivities usually show CO₂/CH₄ selectivities of less than 10–15.¹¹ Chatterjee *et al.* investigated the sour gas permeation properties for several rubbery polymers with selectivities as high as 74 for H₂S/CH₄ (1.3% H₂S feed) for a feed pressure of 14 bar with H₂S molar concentrations of 1.3% and 12.5%. Mohammadi *et al.* studied the acid gas permeation behavior of poly(ester urethane urea) membranes. Although H₂S/CH₄ selectivities of 34 and 43 were achieved for 0.6% H₂S and 3% H₂S feed, respectively, the corresponding moderate CO₂/CH₄ selectivity was only 14. Furthermore, their studies were performed for feed pressures less than 30 bar.³⁰ These conditions are unlikely to reflect the most aggressive

operating conditions in natural gas applications. Because many gas well pressures can reach 50 bar or higher, more aggressive feeds need to be considered, and this is the focus of our work. Feed streams containing both CO₂ and H₂S with relatively high total acid gas concentration and partial pressures require more robust materials capable of removing both acid gases, with stable properties.²⁴

Recently, a number of advanced polymers, including 6FDA-DAM : DABA (3 : 2), and 6FDA-based poly-amide-imides, have been developed for aggressive sour gas separations.^{3,21,22} The goal of the present work was to develop another novel membrane material for the simultaneous removal of H₂S and CO₂ from natural gas under aggressive feed conditions. To the best of our knowledge, intrinsically microporous polyimides have never been applied for sour gas separations. In this paper, we report, for the first time, a novel thermally annealed hydroxyl-functionalized polyimide with intrinsic microporosity (PIM-6FDA-OH) for simultaneous removal of CO₂ and H₂S from natural gas under aggressive feed conditions. Specifically, the performance of PIM-6FDA-OH was tested with high concentrations of H₂S and CO₂ feeds as well as high feed pressures.

Background and theory

Gas permeation

The transport of gases through dense polymeric membranes involves the sorption–diffusion mechanism in which the penetrant first sorbs into the membrane at the upstream feed side, then diffuses across the membrane down a concentration gradient, and finally desorbs from the downstream permeate side. Gas permeation in such cases is characterized by the permeability coefficient, P . As shown in eqn (1), the permeability of a gas i (P_i) is defined as the steady-state flux n_i normalized by the driving partial pressure (Δp_i) across the membrane and the membrane thickness (l).

$$P_i = \frac{n_i l}{\Delta p_i} \quad (1)$$

Permeability is commonly expressed in units of Barrer, where 1 Barrer = 1×10^{-10} (cm³ STP cm cm^{−2} s^{−1} cmHg^{−1}).

In the case of nonideal gas mixtures, an alternative definition of permeability is used to describe the permeation driving force in terms of a fugacity difference rather than a partial pressure difference. For dense films, the fugacity-based permeability, which is used throughout this study, is defined as the flux (n_i), normalized by the transmembrane fugacity driving force of component i (Δf_i) and membrane thickness (l), as shown in eqn (2).

$$P_i = \frac{n_i l}{\Delta f_i} \quad (2)$$

The fugacity coefficients of pure H₂S, CO₂ and CH₄ as well as their state in gas mixtures can be calculated using the Peng–Robinson equation-of-state and the SUPERTRAPP program developed by NIST.²²



Permeability can also be expressed as the product of the effective diffusion coefficient, D , and sorption coefficient, S , of a given gas i within the membrane, as described in eqn (3).

$$P_i = D_i S_i \quad (3)$$

The diffusion coefficient characterizes the kinetic contribution to transport, and the apparent diffusion coefficient D ($\text{cm}^2 \text{s}^{-1}$) of the polymer membrane can be calculated by $D = l^2/6\theta$, where l is the membrane thickness and θ is the time lag as deduced from pure-gas permeability measurements. The sorption coefficient S (cm^3 (STP) cm^{-3} cmHg^{-1}) can then be obtained from the relationship $S = P/D$.

The sorption coefficient represents the thermodynamic contribution to transport, and it can also be measured independently by pressure-decay sorption to allow D to be calculated from $D = P/S$. As shown in eqn (4), for cases with negligible downstream pressure, the sorption coefficient can be expressed as:

$$S_i = \frac{c_i}{f_i} \quad (4)$$

where c_i is the concentration of a gas sorbed in the membrane, and f_i is the corresponding upstream fugacity driving force of component i . For glassy polymers, this relationship is often described by the dual-mode sorption model, which is given as:^{31,32}

$$c_i = c_{D,i} + c_{H,i} = k_{D,i}f_i + \frac{C'_{H,i}b_i f_i}{1 + b_i f_i} \quad (5)$$

where $c_{D,i}$ is the Henry's law or dissolved mode penetrant concentration, $c_{H,i}$ is the penetrant concentration in the Langmuir mode or hole-filling sorption mode. In eqn (5), $k_{D,i}$ is the Henry's law sorption coefficient, $C'_{H,i}$ is the Langmuir capacity constant, and b_i is the Langmuir affinity constant. As with permeability, fugacity (f_i) values are substituted in place of pressure values to connect more directly to the true thermodynamic properties of the penetrants.

Koros *et al.* extended the dual-mode sorption model represented by eqn (5) to account for competition in binary gas mixtures at concentrations below which swelling induced complications occur.^{33,34} Recently, this dual-mode model was used for ternary mixed gas feed cases by Kraftschik *et al.*²⁴ The ternary mixed gas dual-mode sorption model for components A, B and C can be given in eqn (6)–(8).

$$c_A = k_{D,A}f_A + \frac{C'_{H,A}b_A f_A}{1 + b_A f_A + b_B f_B + b_C f_C} \quad (6)$$

$$c_B = k_{D,B}f_B + \frac{C'_{H,B}b_B f_B}{1 + b_A f_A + b_B f_B + b_C f_C} \quad (7)$$

$$c_C = k_{D,C}f_C + \frac{C'_{H,C}b_C f_C}{1 + b_A f_A + b_B f_B + b_C f_C} \quad (8)$$

The ideal selectivity between the fast gas (i) and slow gas (j), defined as the ratio of permeabilities (eqn (9)), equals the mixed-gas “separation factor” (eqn (10)) when the downstream

pressure is negligible compared to the feed pressure, as valid in the current study.

$$\alpha_{i/j} = \frac{P_i}{P_j} = \frac{D_i}{D_j} \frac{S_i}{S_j} = \alpha_D \alpha_S \quad (9)$$

where α_D is the diffusivity or mobility selectivity and α_S is the sorption selectivity. Moreover, for actual mixed gas feeds,

$$\alpha_{i/j} = \frac{(y_i/y_j)}{(x_i/x_j)} \quad (10)$$

where y_i is the mole fraction of component (i) on the permeate side, and x_i is the mole fraction of component (i) on the feed side of the membrane, as measured by gas chromatography (GC).

Experimental

Materials

As noted earlier,³⁵ the monomer 4,4'-(hexafluoroisopropylidene) diphthalic anhydride (6FDA, 99%) was obtained from Aldrich and purified by sublimation before use. *N*-Methylpyrrolidone (NMP) was refluxed over P_2O_5 for 4 h before vacuum distillation and, thereafter, stored over 4 Å molecular sieves. Pyridine was distilled freshly prior to use. Bisphenol A, methylsulfonic acid, dichlorotin hydrochloride acid solution, sodium carbonate, tetrahydrofuran, dichloromethane, ethyl acetate, ligroin, acetic acid, and nitric acid were obtained from Aldrich and used as received. CO_2 and CH_4 with 99.999% purity were obtained from Airgas, whereas H_2S was obtained from Praxair with 99.6% purity. The ternary gas mixture used was also obtained from Praxair with a composition of 15 vol% H_2S , 15 vol% CO_2 , and 70 vol% CH_4 .

Synthesis of PIM-6FDA-OH

The pristine polymer PIM-6FDA-OH was synthesized according to the previously reported method.³⁵ Briefly, the diamine monomer, 3,3',3'-tetramethyl-1,1'-spirobisindane-5,5'-diamino-6,6'-diol, with *o*-OH groups was first synthesized. 4,4'-(Hexafluoroisopropylidene) diphthalic anhydride (6FDA) was then reacted with the diamine monomer for polymerization *via* a solvothermal azeotropic imidization reaction. In this way, the hydroxyl-functionalized PIM-structured polyimide (PIM-PI) was obtained, which is denoted here as PIM-6FDA-OH. The chemical structure of PIM-6FDA-OH is shown in Fig. 1. This rigid polymer does not show a true glass transition temperature, and it degrades at high temperature ($>380^\circ\text{C}$). Note that the presence of the polar OH group in PIM-6FDA-OH provides added cohesive forces to stabilize the matrix against acid gas plasticization.

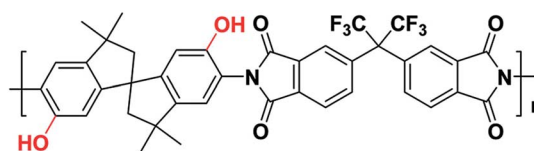


Fig. 1 Chemical structure of the PIM-6FDA-OH polymer.



Fortunately, it is the standard procedure to remove moisture from natural gas feeds to produce noncorrosive dry gases with low “dew points”. This fact eliminates possible concern regarding the hydrophilicity of the PIM-6FDA-OH.³⁶

Membrane fabrication

The polymer (PIM-6FDA-OH) was dissolved in THF to form a 3–5 wt% polymer solution and placed on a roller for at least 24 h for mixing, then purified using 1.0 μm PTFE filter cartridges. The polymer solution was used to prepare polymer dense films by a solution casting method in a glove bag at room temperature to achieve slow evaporation (3–4 days) and the vitrified films were then removed and dried in a vacuum oven at 120 °C for at least 12 h to remove residual solvent. Finally, the films were thermally annealed at 250 °C for 24 h under high vacuum. This annealing step has been shown earlier in studies with CO₂ and CH₄ to stabilize the polymer matrix against plasticization.³⁷ The thicknesses and effective areas of the films were measured using a digital micrometer and image processing software, respectively.

Permeation measurements

Pure and mixed gas permeation experiments were performed using H₂S, CO₂, and CH₄ as well as a ternary mixture of these three components. While there are few studies reported on H₂S-containing feeds, for the aggressive feeds considered here, a special facility was needed. The detailed description of this facility is provided in reference, which is available electronically on the link <http://hdl.handle.net/1853/50289>.³⁸ Nevertheless, a short summary of the key procedures followed is provided. Dense film permeation was conducted at 35 °C using a previously described constant volume/variable pressure permeation apparatus.^{39–41} The membranes were degassed in the permeation system on both sides under high vacuum at 35 °C for at least 24 h before any permeation test. Several modifications were made to the standard permeation system design to ensure safety when handling H₂S and high concentration H₂S gas mixtures.^{4,22} The permeation cell was additionally enclosed in a large ventilated cabinet as a secondary compartment to prevent H₂S exposure if a leak was to occur in the system. In addition, two pneumatically actuated valves were used in place of standard hand-operated valves and controlled by a Labview® program for additional safety. In addition, the downstream-actuated valve was programmed to shut down when the downstream pressure reached a certain maximum pressure to avoid over-pressurization that may damage the pressure transducers, and also to prevent unintended release of large quantities of H₂S and minimize operator risk when handling H₂S.

To measure permeability, the gas was first introduced on the feed side and allowed to fill a ballast volume. The pneumatically actuated valve was then opened on the Labview® program to feed the membrane on the upstream side. As the gas permeated through the membrane to the downstream (permeate) side, the increase in pressure with time was recorded using the Labview® program until steady-state was reached. To ensure attainment of true steady state, the total flux was monitored until a constant

value was achieved and then compositional steady state was verified. Specifically, not only was it verified that the total flux was constant, but also that the mole fraction composition of the various components contributing to the total flux was constant. As a practical matter, the attainment of total flux steady state and permeate compositional steady state coincided. This fact notwithstanding the achievement of steady state exceeded the expected time based on sample Fickian transport. Nevertheless, once steady state was achieved, it was stable. The upstream pressure was maintained constant throughout the experiment and also recorded using Labview®. A downstream pressure *vs.* time plot was then generated using the collected data. A Varian 450-GC was used during mixed gas permeation experiments to determine the permeate gas composition. The feed pressure and retentate flow were maintained by keeping the stage cut below 1% using an ISCO syringe pump and a metering valve. The syringe pump was maintained at constant pressure and the gas was fed at the same rate as the retentate vented through the metering valve. A low stage cut was used to: (i) prevent concentration polarization on the upstream side and (ii) maintain essentially a constant feed and residue concentration in order to provide a constant driving force across the membrane during the experiment. A high-temperature epoxy, Duralco™ 4525 (Cotronics Corp.), was used on all samples to seal the membrane-tape masking interface. This was done to prevent delamination of the masked films, which has been observed with less durable sealing epoxies when using highly sorbing species such as CO₂ and, in particular, H₂S.²²

Pure gas sorption

Pure gas sorption experiments were performed with H₂S, CO₂, and CH₄. A pressure decay sorption apparatus was used to measure the sorption isotherms of the PIM-6FDA-OH dense film at 35 °C.⁴² These systems have been described in detail elsewhere, but a few minor alterations were made to ensure operator safety when experimenting with H₂S.^{4,22} The density of the polymer was determined gravimetrically by its measured weight, area, and film thickness.³⁵ The density measurement was used to calculate the fractional free volume of the polymer and the sorption capacities.

Results and discussion

Pure gas permeation

Pure gas permeation experiments were performed on the thermally annealed PIM-6FDA-OH films using H₂S, CO₂, and CH₄ at 35 °C with the constant-volume/variable-pressure apparatus, previously mentioned for handling H₂S gas mixtures.⁴ Both low and high pressures were studied to compare the transport properties of these annealed films with values reported in the previous literature.³⁵ All permeability calculations used the fugacity driving force definition of dense film permeability that has been reported for highly aggressive feed streams, such as those with elevated CO₂ or H₂S levels.²² The permeability was calculated from the steady-state region of the downstream pressure–time curve, and the diffusion coefficient (*D*) was



determined by the time-lag method. The pure gas results of the thermally annealed PIM-6FDA-OH films and other polymer materials were plotted on permeability–selectivity trade-off curves^{12,13} for CO₂/CH₄ in Fig. 2 and H₂S/CH₄ in Fig. 3. It can be seen from Fig. 2 that the PIM-6FDA-OH membranes are more permeable than conventional OH-functionalized polyimides owing to the microporosity introduced by the spiro-induced contorted structure of the polymer. For example, the CO₂ permeability coefficient of the thermally annealed PIM-6FDA-OH film in this work is 149 Barrers, whereas conventional OH-containing polyimides typically have CO₂ permeabilities of less than 20 barrers.⁴³ As shown in Fig. 2, the thermally annealed PIM-6FDA-OH films have much higher CO₂/CH₄ selectivity than traditional PIM-1 and PIM-PIs. Because a H₂S/CH₄ upper bound plot does not exist yet in the literature due to the limited amount of data available for this gas pair, we only show our current polymer performance relative to other reported data. As shown in Fig. 3, the thermally annealed PIM-6FDA-OH film has a reasonable H₂S/CH₄ selectivity and shows much higher H₂S permeability than other glassy polymers such as CA, 6F-PAI, and 6FDA-DAM-DABA (3 : 2), similar to the PEG crosslinked 6FDA-DAM-DABA (PEGMC) material reported earlier,²⁴ indicating that the PIM-6FDA-OH material is very promising for sour gas separations.

Pure gas sorption

Sorption measurements for the sour gas components were performed on thermally annealed PIM-6FDA-OH films using the pressure decay method^{42,46} at 35 °C. The films were dried in a vacuum oven at 100 °C for at least 12 h prior to testing to remove any moisture. The sample cell was then evacuated for 2 days prior to testing and evacuated for 24 h at the completion of each gas isotherm. The results of H₂S, CO₂ and CH₄ pure gas sorption experiments are shown in Fig. 4. The “dual-mode” sorption model with both Langmuir (hole-filling) and Henry's law (dissolution) is apparent in the concave sorption isotherms. The

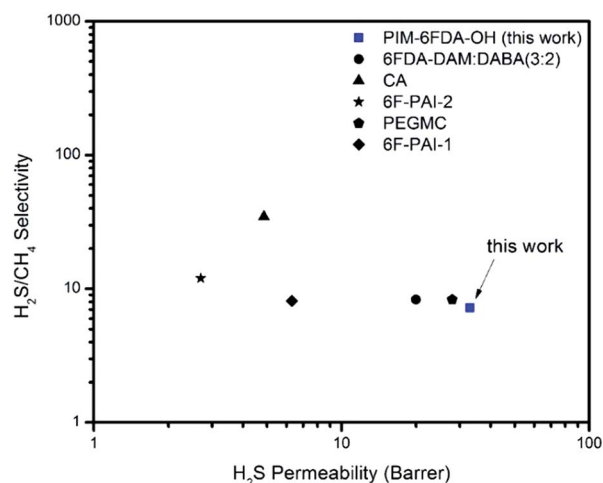


Fig. 3 H₂S/CH₄ permeability–selectivity trade-off comparison of thermally annealed PIM-6FDA-OH to other polymers materials^{3,4,22,24} in pure-gas feeds at 4.5 bar and 35 °C.

dual-mode sorption model was then fitted using the least-squares method to the dual-mode sorption equation to each of the sorption isotherms to give dual-mode sorption parameters. Good agreement between the model and the sorption data was achieved over the pressure range tested. It should be noted here at higher pressures, H₂S swelling in GCV-modified CA and 6FDA-DAM-DABA (3 : 2) was apparent and marked by a deviation from the dual-mode fit, *which was not observed for the thermally annealed PIM-6FDA-OH films*.^{22,24} Table 1 shows the best-fit dual-mode parameters for the thermally annealed PIM-6FDA-OH material and some other glassy polymers for H₂S, CO₂ and CH₄ sorption.

As shown in Table 1, the Henry's law sorption coefficients of H₂S and CO₂, k_D , for the thermally annealed PIM-6FDA-OH film are significantly lower than those of 6FDA-DAM : DABA (3 : 2) and crosslinked TEGMC. This may be due to the higher polarity

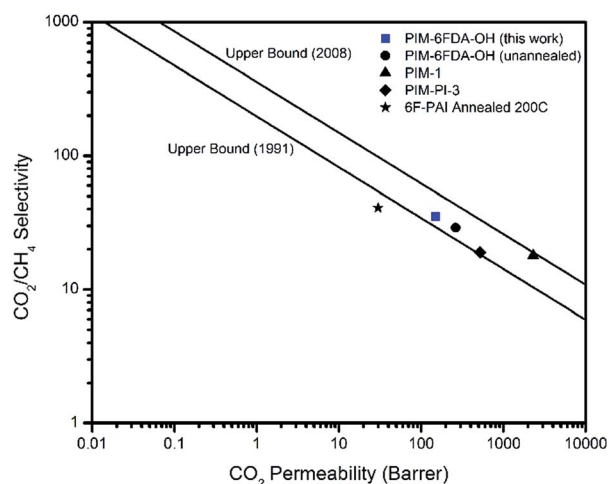


Fig. 2 CO₂/CH₄ permeability–selectivity trade-off curve^{12,13} comparison of thermally annealed PIM-6FDA-OH to other polymers materials^{3,35,44,45} in pure-gas feeds at 35 °C.

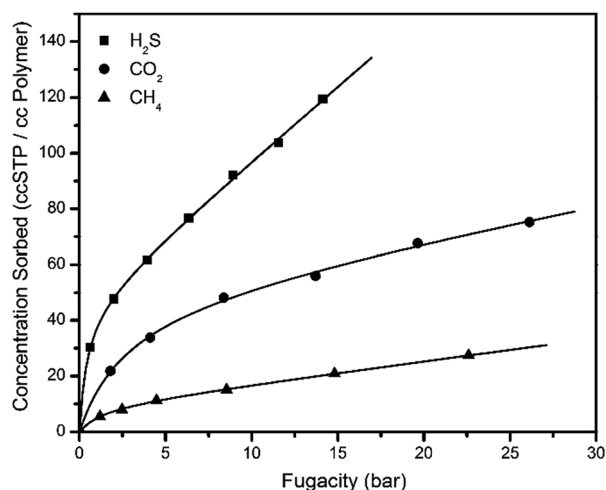


Fig. 4 Pure gas (H₂S, CO₂, and CH₄) sorption isotherms and dual-mode model fit of thermally annealed PIM-6FDA-OH at 35 °C.



Table 1 Dual-mode sorption model parameters for pure H₂S, CO₂ and CH₄^a

Polymer	H ₂ S			CO ₂			CH ₄		
	<i>k_D</i>	<i>C'_H</i>	<i>b</i>	<i>k_D</i>	<i>C'_H</i>	<i>b</i>	<i>k_D</i>	<i>C'_H</i>	<i>b</i>
PIM-PMDA-OH	5.28	45.9	2.19	1.52	45.7	0.40	0.81	9.63	0.72
6FDA-DAM : DABA (3 : 2) ^b	9.55	38.1	3.81	2.39	44.0	0.72	0.06	27.2	0.19
TEGMC ^c	7.16	38.7	2.87	2.34	37.0	0.87	0.27	27.9	0.13

^a *k_D* [cm³ (STP) cm⁻³ bar⁻¹], *C'_H* [cm³ (STP) cm⁻³], *b* [bar⁻¹]. ^b Data from ref. 22. ^c Data from ref. 24.

of H₂S, whose sorption depends more on physiochemical interactions with the polymer than simply free volume within the matrix. However, PIM-6FDA-OH gives a significantly higher Henry's law parameter, *k_D*, for CH₄, indicating that non-polar CH₄ sorption depends more on free volume within the matrix rather than physiochemical interactions with the polymer. Table 1 also shows that the total sorption capacity of the lower-density regions (unrelaxed gaps), characterized by the Langmuir capacity constants, *C'_H*, of both H₂S and CO₂ in the PIM-6FDA-OH are slightly higher than those of the other polymers, which is consistent with higher fractional free volume of PIM-6FDA-OH compared to the other materials.

To obtain insight into gas sorption levels under mixed gas feed conditions that correspond to the mixed gas permeation tests performed in this work, mixed gas sorption values were estimated using the dual-mode sorption parameters for H₂S, CO₂ and CH₄ recorded in Table 1 according to eqn (6)–(8). Fig. 5 shows the predicted mixed gas sorption values for H₂S, CO₂ and CH₄ at 35 °C with a 15% H₂S, 15% CO₂, and 70% CH₄ feed mixture in the thermally annealed PIM-6FDA-OH material. Calculations were also performed with the crosslinked TEG-modified PEGMC material for comparison, and the corresponding dual-mode sorption parameters were taken from ref. 24. It can be seen that the gas sorption values for H₂S, CO₂ and CH₄ are predicted to show a decrease in solubility in the mixture. Compared with the crosslinked PEGMC material, both H₂S and CO₂ sorption in the thermally annealed PIM-6FDA-OH material experienced a significant reduction under mixed gas feed conditions due to lower Langmuir affinity constant values. This affinity coefficient is an equilibrium constant equal to the ratio of solute sorption and desorption rate constants from the Langmuir sites,³² associated with H₂S and CO₂. However, the difference of CH₄ sorption between the pure- and mixed-gas sorption isotherms in the thermally annealed PIM-6FDA-OH material was much smaller than that in the crosslinked PEGMC material due to a relatively high CH₄ Langmuir affinity constant value in the PIM-6FDA-OH. This is currently not well understood, but based on the mixed gas sorption predictions, it is very clear that strong competitive sorption effects should exist in these sour gas separation systems. Although the mixed gas sorption calculations in this work are a good starting point, further research on mixed gas sorption experiments corresponding to mixed gas permeation tests would be a more useful approach for evaluating membrane performance for realistic sour gas separations. This approach may provide direct insight into how the material structure relates to competitive sorption

under practically relevant operating conditions. Unfortunately, these tests were beyond the scope of the current work and we are not currently able to make direct mixed gas sorption measurements.

The pure H₂S, CO₂, and CH₄ permeation isotherms for the PIM-6FDA-OH dense films at 35 °C are shown in Fig. 6–8. It can be seen that no H₂S-induced plasticization of the PIM-6FDA-OH film occurs in a pure H₂S feed at 35 °C up to 4.5 bar feed pressure, and only a slight plasticization is observed above 4.5 bar of pure H₂S. This can be explained by accelerated chain relaxation and reduced free volume in the annealed samples. In our previous studies on the annealing effect on the 6FDA-DAM : DABA (3 : 2) polymer, the results showed that the annealed films exhibit non-negligible plasticization pressures.²² Increasing the annealing temperature from 180 °C to 230 °C caused an increase in the H₂S plasticization pressure of approximately 25% to a value of 2.5 bar.

Similarly, the hydroxyl-functionalized PIM films indicated significant improvement in CO₂ plasticization resistance up to 28 bar feed pressure (Fig. 7). Carbon dioxide showed a higher resistance to swelling due to its lower sorption, caused by its lower critical temperature compared to H₂S. In comparison, for the unannealed PIM-6FDA-OH films, CO₂-induced plasticization occurred at ~6.9 bar.³⁵ In addition to the increased plasticization resistance in the annealed films, the CO₂ permeability of annealed PIM-6FDA-OH films decreased. Presumably, this is again due to accelerated chain relaxation and lower free volume effects caused by sub-*T_g* annealing.²² Swelling-induced plasticization is a common phenomenon for polymer membranes in gas separations involving aggressive feed streams, such as CO₂ and H₂S in sour gas.⁴ Plasticization occurs when a penetrant significantly increases the mobility of polymer chain segments, thereby increasing the diffusion coefficients of all penetrants in the membrane. Penetrant molecules with higher critical temperatures like H₂S and CO₂ are more capable of inducing swelling, because they have a considerably higher sorption capacity, particularly in glassy polymers.^{4,8,22,24} As shown in Fig. 8, methane does not plasticize at any of the pressures investigated.

As discussed in the theory section, the permeability coefficient is defined as the product of the diffusion coefficient and the sorption coefficient; therefore, the selectivity can be decoupled into diffusion and sorption selectivity. To better understand the role of hydroxyl groups in H₂S/CH₄ and CO₂/CH₄ selectivity, diffusion coefficients (*D*) and solubility coefficients (*S*) were measured using both the time-lag permeation



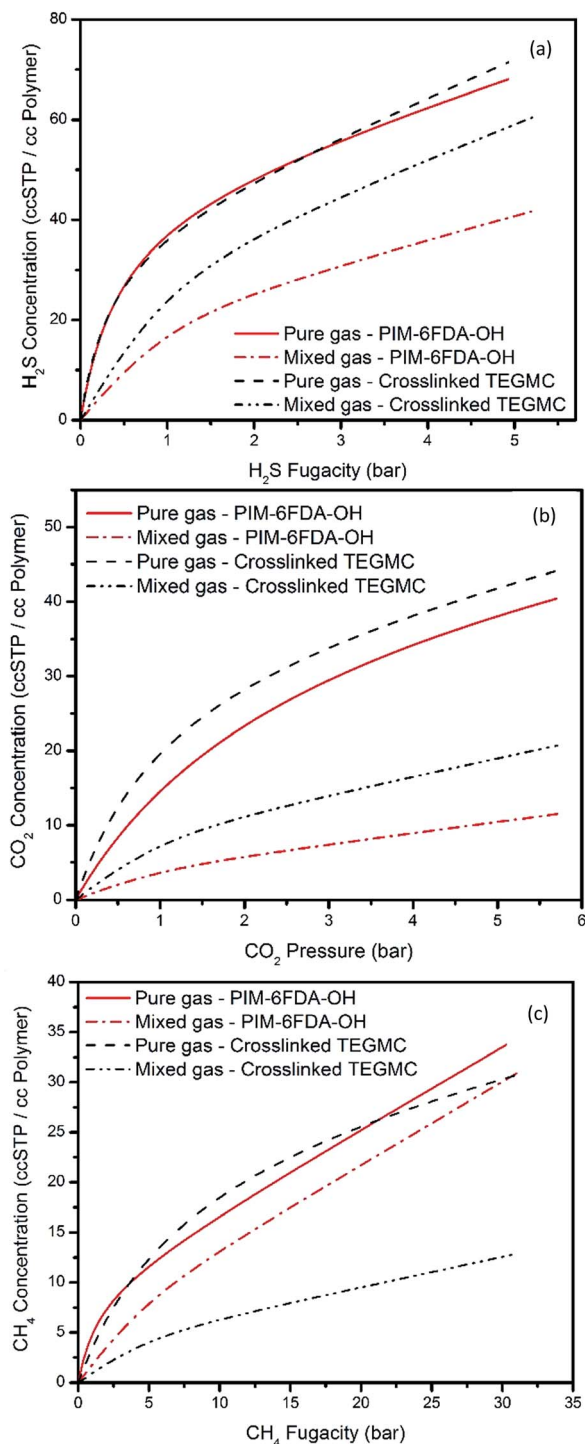


Fig. 5 Sorption isotherms at 35 °C for the thermally annealed PIM-6FDA-OH and cross-linked PEGMC films with TEG as the cross-linking agent. Pure gas dual-mode sorption model fits are plotted along with mixed gas sorption predictions for a 15% H₂S, 15% CO₂, and 70% CH₄ feed mixture. The dual-mode sorption model best fit parameters of cross-linked PEGMC are adapted from ref. 24 and used for calculations.

method and pressure-decay sorption method (Fig. 4). Using the permeation and sorption results, the kinetic (diffusion) and thermodynamic (sorption) individual contributions of the

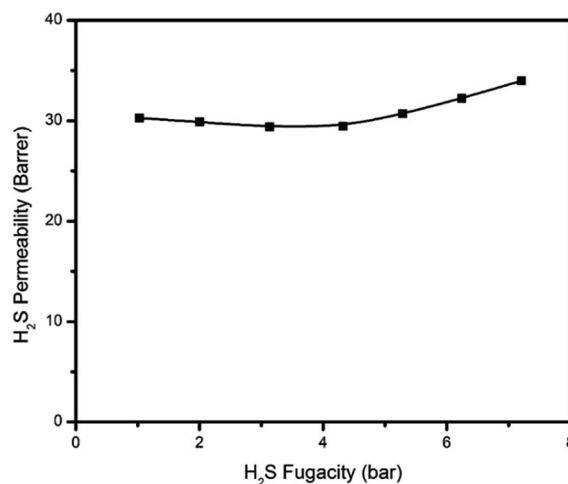


Fig. 6 Pure H₂S permeability isotherm for an annealed PIM-6FDA-OH film at 35 °C.

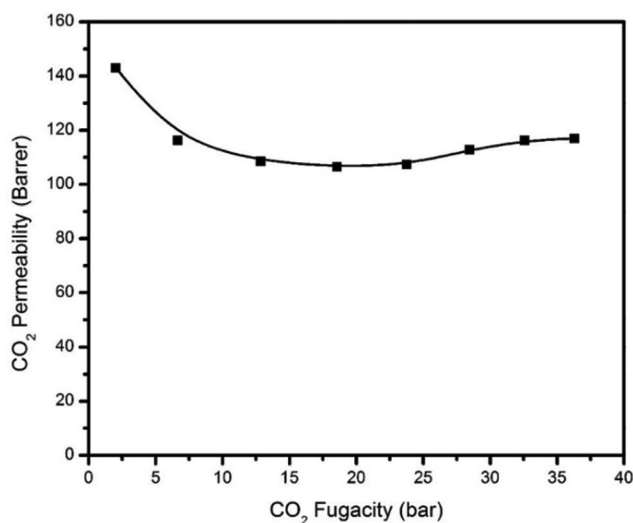


Fig. 7 Pure CO₂ permeability isotherm for an annealed PIM-6FDA-OH film at 35 °C.

thermally annealed PIM-6FDA-OH and the comparison to other polymers were calculated and are shown in Table 2. It can be seen that the D and S values determined from the two methods are in good agreement. Despite the lower diffusion coefficients of functionalized PIM-6FDA-OH, it shows much higher CO₂/CH₄ diffusion selectivity in comparison with PIM-1 and PIM-PI-3, which is more typical for a glassy polymer, with diffusion selectivity as the major contributor to overall permselectivity.²² Benefitting from the PIM segments in the molecular structure, the OH-functionalized polymers reported in this study showed increased CO₂/CH₄ selectivity while maintaining high permeability in comparison with traditional PIMs and PIM-PIs. It can also be seen from Table 2, the H₂S/CH₄ selectivity of the thermally annealed PIM-6FDA-OH is primarily derived from the solubility contribution despite the fact that it is a glassy material. Because H₂S has a smaller kinetic diameter than CH₄ and



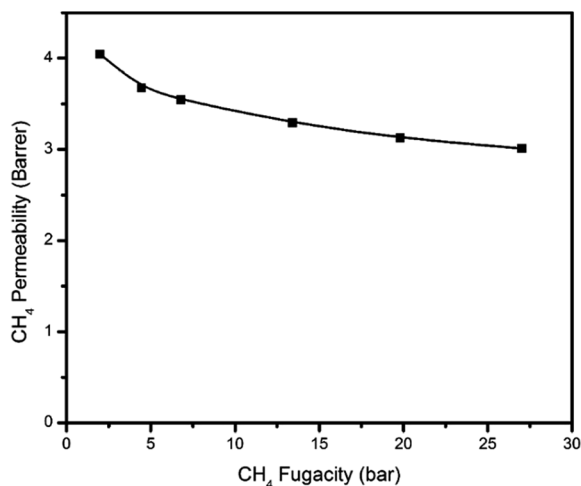


Fig. 8 Pure CH₄ permeability isotherm of an annealed PIM-6FDA-OH film at 35 °C.

should be diffusion-favored, this result suggests that strong polymer-H₂S interactions decrease the diffusion coefficient of H₂S in the membrane. Similar results were observed in our previous research on 6F-PAI and 6FDA-DAM-DABA (3 : 2) materials.^{21,22}

Mixed gas permeation

Although the thermally annealed PIM-6FDA-OH film showed very promising results in pure gas feeds (Fig. 2 and 3), multi-component mixture tests are more practical to assess its true performance. In this study, ternary gas permeation measurements were made with a 15% H₂S, 15% CO₂ and 70% CH₄ mixture at upstream pressures ranging from 7 to 48 bar and with vacuum downstream. Fig. 9(a–c) show the H₂S, CO₂, and CH₄ permeabilities of thermally annealed PIM-6FDA-OH films in the ternary mixture, while Fig. 10(a) and (b) show the H₂S/CH₄ and the CO₂/CH₄ selectivities, respectively.

As shown in Fig. 9, it is very clear from the CH₄ and CO₂ permeability isotherms for PIM-6FDA-OH films that

plasticization did not occur even at high acid gas partial pressures. However, severe H₂S-induced plasticization effects were evident at the highest feed pressure of 48 bar. This is expected due to the very high condensability of H₂S and its capacity to form polymer-penetrant interactions with the polymer backbone. It is somewhat surprising that despite the plasticization apparent for H₂S, CO₂ and CH₄ as co-penetrants do not show apparent increases in permeabilities for the same mixed gas feed. Similar results were observed in our previous studies using 6FDA-DAM-DABA (3 : 2) and CA materials.^{4,22,24} Again, as shown in Fig. 6, in pure gas feed, H₂S-induced plasticization of the thermally annealed PIM-6FDA-OH film did not occur until the H₂S feed pressure was higher than 4.5 bar (only a slight change even at 8 bar), which means the annealed PIM-6FDA-OH film has a much less pronounced plasticization response. Clearly, the plasticization/swelling effects under aggressive conditions that caused a reduction of CO₂/CH₄ selectivity to about 15 (unpublished data) in non-annealed films were significantly minimized in the films annealed at 250 °C. Interestingly, Fig. 10 shows that when the CO₂/CH₄ selectivity decreases, the H₂S/CH₄ selectivity increases with increasing feed pressure. This is because in a ternary system, the highly condensable gases, CO₂ and H₂S, now have to compete for the Langmuir sorption sites.⁴ Because H₂S has a higher affinity for these sorption sites, the sorption capacity of CO₂ is presumably greatly reduced. This leads to a decrease of CO₂ permeability whereas an increase of H₂S permeability is observed. Methane is not greatly affected in this case because it already has lower affinity for the Langmuir sorption sites than both CO₂ and H₂S, which shows a similar trend to cellulose acetate and thermally annealed 6FDA-DAM-DABA (3 : 2) films.^{4,22} It should be noted that at the high end of the pressure range (48 bar), the H₂S/CH₄ selectivity reached nearly 30 in the thermally annealed PIM-6FDA-OH film, which is much higher than most other glassy polymers (~15) and is very competitive compared with rubbery polymers. More interestingly, the CO₂/CH₄ selectivity (~25) suffers less significant loss *versus* the non-annealed sample, indicating the thermally annealed OH-functionalized spiro-polyimides in

Table 2 Diffusion coefficient (*D*), solubility coefficient (*S*), diffusion selectivity (α_D), and solubility selectivity (α_S) of PIMs-6FDA-OH and other polymers at 35 °C

Polymer	<i>D</i> (10 ^{−8} cm ² s ^{−1})			<i>S</i> (10 ^{−2} cm ³ (STP) cm ^{−3} cmHg ^{−1})			α_D		α_S	
	CH ₄	CO ₂	H ₂ S	CH ₄	CO ₂	H ₂ S	CO ₂ /CH ₄	H ₂ S/CH ₄	CO ₂ /CH ₄	H ₂ S/CH ₄
PIMs-6FDA-OH ^a	0.844	8.92	0.637	4.98	16.7	46.4	10.6	0.75	3.35	9.3
PIMs-6FDA-OH ^b	0.868	9.61	0.599	4.84	15.5	49.3	11.1	0.69	3.20	10.2
PIMs-6FDA-OH ^c	2.02	9.88	—	4.51	26.7	—	4.89	—	5.92	—
PIM-1 ^d	6.8	26	—	18	88	—	3.82	—	4.89	—
PIM-PI-3 ^e	3	12	—	9.3	44	—	4.0	—	4.73	—
CA ^f	0.21	0.86	0.34	0.62	4.93	14.0	4.09	1.63	7.99	22.7
Crosslinked PDMC ^g	0.82	7.18	1.07	2.79	12.2	20.9	8.70	1.29	4.37	7.49

^a *D* is determined by the constant volume time-lag method; *S* is deduced based on the equation $P = DS$. ^b *S* is measured by pressure-decay sorption; *D* is calculated from $P = DS$. ^c Data from ref. 35. ^d Data from ref. 44. ^e Data from ref. 45. ^f Data from ref. 4. ^g Data from ref. 38.



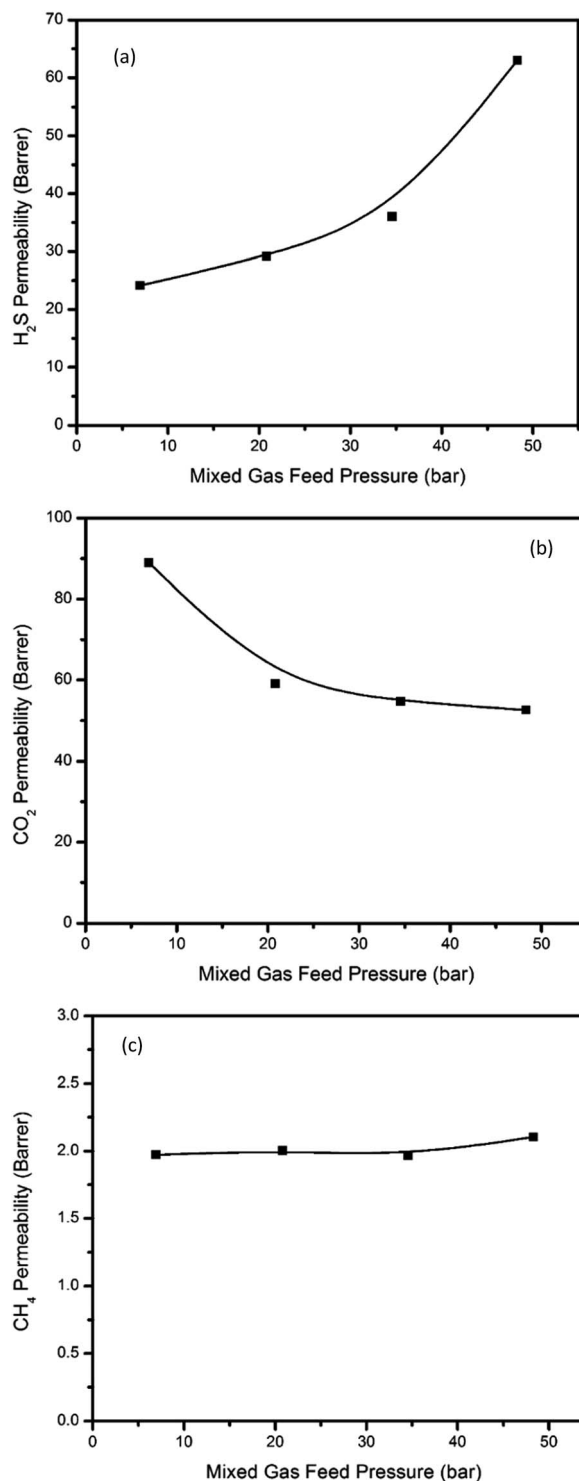


Fig. 9 Mixed gas (15% H₂S, 15% CO₂, 70% CH₄) permeabilities in PIM-6FDA-OH films at 35 °C.

this study plasticized significantly less as compared to conventional non-crosslinked 6FDA-based polyimides. This unique performance at high pressures is very impressive, since most literature reports on rubbery polymers, which generally show very high H₂S/CH₄ selectivity, were determined only at low H₂S concentrations and low pressures.

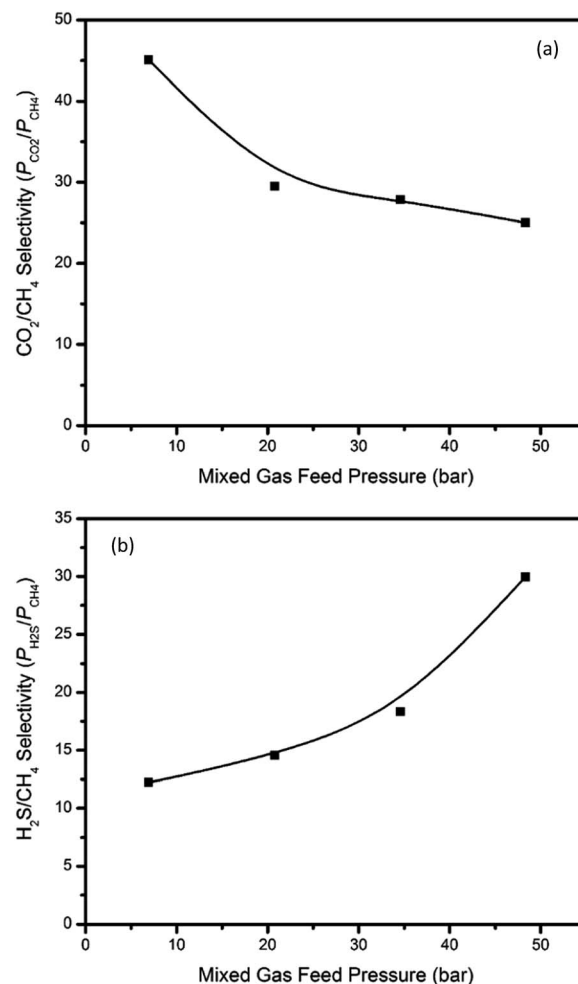


Fig. 10 Mixed gas (15% H₂S, 15% CO₂, 70% CH₄) selectivities for acid gases of PIM-6FDA-OH at 35 °C.

Pure and mixed gas permeation modeling

The partial immobilization model (dual-mode extension) and dual-mode sorption parameters for each gas can be used in the predictions of pure gas permeation values in the absence of plasticization or swelling or swelling induced bulk flow effects.³⁴ The above coefficients are deceptively simple in appearance; however, depending on the assumptions made, their interpretation can be complex. To enable readers to understand these issues, we have provided details in the ESI,[†] while presenting the key results of these detailed analysis in summary form here. Fig. 11 shows the experimental permeability data as well as the partial immobilization model predictions for pure H₂S, CO₂, and CH₄ permeability through the thermally annealed PIM-6FDA-OH film. These curves indicate good agreement between the measured permeation data and the model predictions prior to the point at which H₂S- and CO₂-induced plasticization occurs and within the entire CH₄ permeability isotherm.

Permeation modeling based on dual-mode transport through glassy polymers can also be extended to mixed gases (eqn S5 in the ESI[†]).³⁴ Because the dual-mode model parameters are calculated based on pure gas permeation and sorption data,



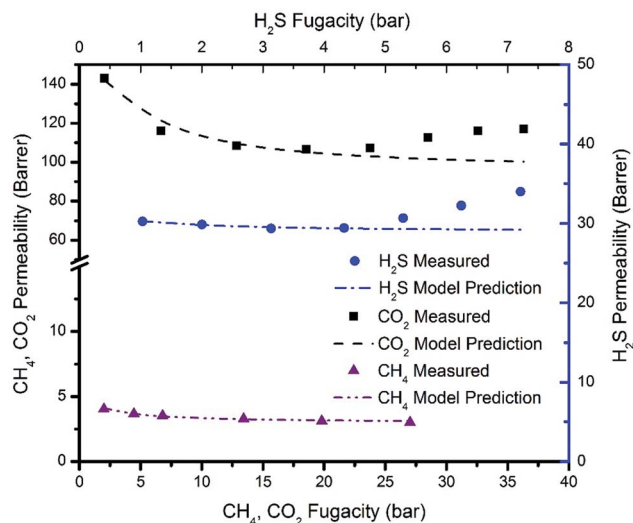


Fig. 11 Partial immobilization model projections for pure H_2S , CO_2 and CH_4 permeability at 35°C in the thermally annealed PIM-6FDA-OH films.

deviations between mixed gas experimental permeation data and model predictions can be observed in some cases, especially for mixed gas feeds that lead to significant polymer-penetrant interactions or other effects that are not accounted for in the model. More complex models should be used in these cases. For instance, the so called “frame of reference” (or bulk flow) model can be used to account for bulk (convective) flux through the membrane (eqn S12–S22 in the ESI†). The bulk flux contribution usually becomes non-negligible under mixed gas feed conditions, especially when highly condensable species (like CO_2 and H_2S) are present. The detailed interpretation of these models and difference for the various penetrants are provided in the ESI.†

The dual-mode and frame of reference models were applied for permeation predictions for a 15% H_2S , 15% CO_2 , and 70% CH_4 mixed gas feed with the thermally annealed PIM-6FDA-OH films. The results are shown in Fig. 12 and 13. The predicted permeability and permselectivity values given by both models (especially the more complicated frame of reference model with bulk flux contributions) are in close agreement with the experimental values for some cases for binary mixtures in the literature.^{34,47–49} For the current case, however, it is clear from the permeability and permselectivity calculations shown in Fig. 12 and 13 that the presence of H_2S in the feed mixture adds unexpected complexity to the system. The permeability and permselectivity values given by *both models* are quite poor in capturing the experimentally observed trends, *even when the frame of reference is accounted for in the bulk flow model*. The experimental permeability values for CO_2 and CH_4 are far below the model predictions, whereas H_2S experimental values are well above the model predictions at higher feed pressures. Additionally, the predicted $\text{H}_2\text{S}/\text{CH}_4$ permselectivities are far below the measured values, while the measured CO_2/CH_4 permselectivities are well above the predicted value at lower feed pressure, although the frame of reference model can

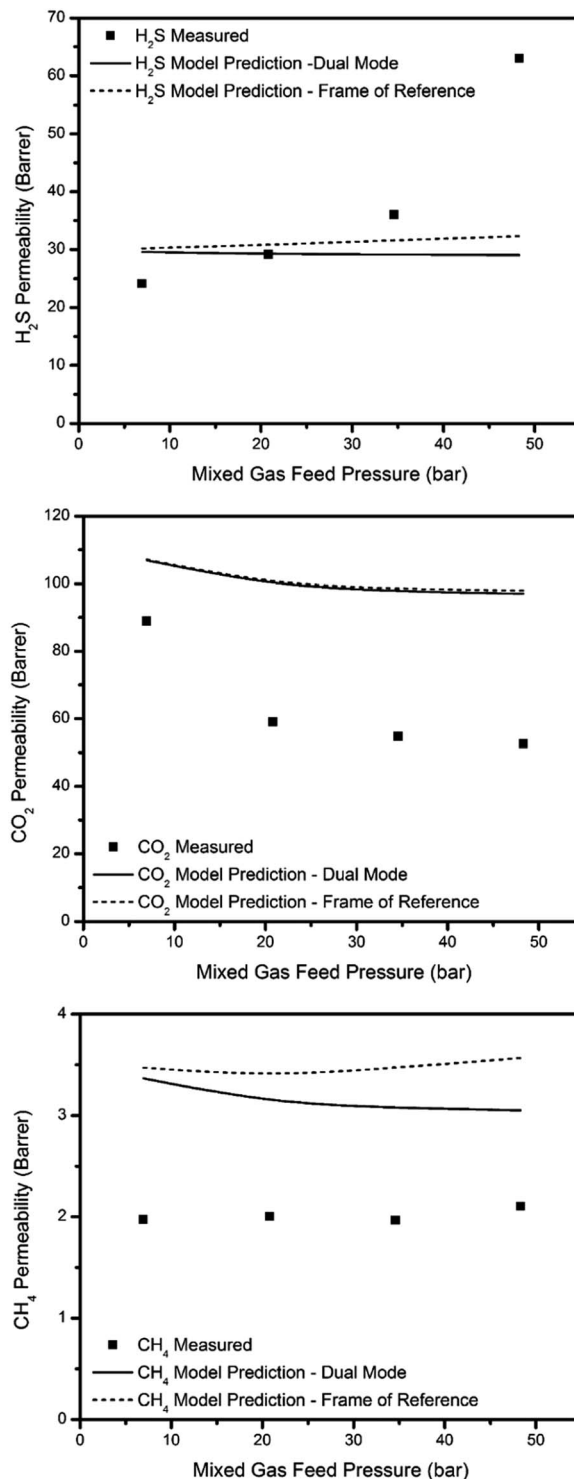


Fig. 12 Model predictions for H_2S , CO_2 , and CH_4 permeability of a 15% H_2S , 15% CO_2 , and 70% CH_4 mixed gas feed with thermally annealed PIM-6FDA-OH films.

describe the CO_2/CH_4 permselectivities fairly well at the higher feed pressures. It is interesting to note that the frame of reference model gives significantly different predictions for permeability of H_2S and CH_4 , and CO_2/CH_4 permselectivity than the simpler dual-mode model, however, the predictions in both



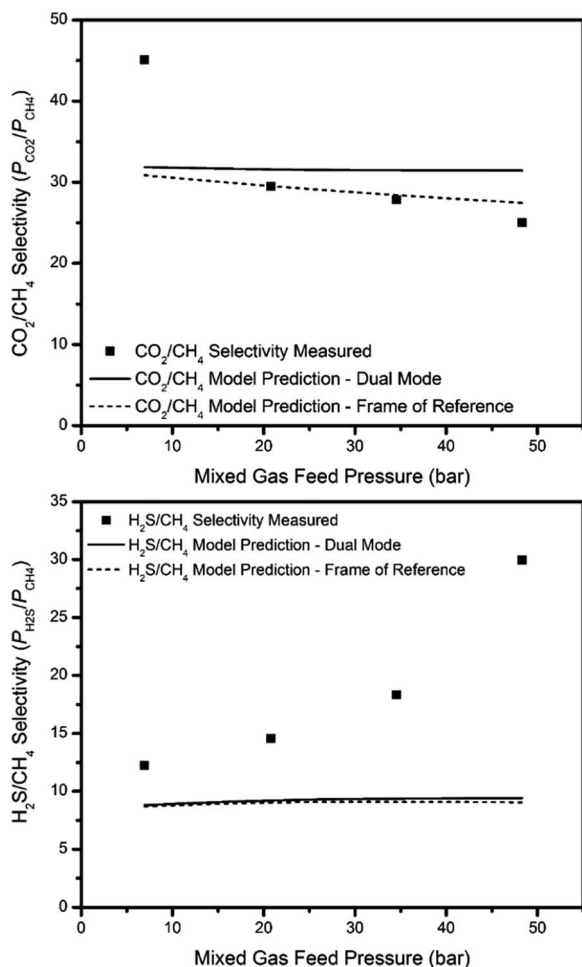


Fig. 13 $\text{H}_2\text{S}/\text{CH}_4$ and CO_2/CH_4 permselectivity projections for 15% H_2S , 15% CO_2 , and 70% CH_4 mixed gas feed at 35 °C.

cases are rather poor. Although at this time it is not possible to identify the exact transport mechanism leading to the poor agreement between observed permeation results and model projections in ternary mixtures containing H_2S , it clearly deserves further investigation. Future work in this area will include considerations of models that may address the two models considered here for sour gas permeation performance of the glassy polymers used in this work.

Table 3 summarizes most of the mixed gas studies that have been conducted on polymeric dense films for sour gas separations. It is clear that the performance of the thermally annealed PIM-6FDA-OH films is very impressive compared to most other polymers shown in this table. The $\text{H}_2\text{S}/\text{CH}_4$ selectivity is 30 at 48 bar, which is much higher than most other glassy polymers, and H_2S permeability is also much higher than cellulose acetate, 6FDA-DAM : DABA (3 : 2) and novel 6FDA-PAI materials.²¹ Even compared with rubbery polymers, PIM-6FDA-OH still shows competitive $\text{H}_2\text{S}/\text{CH}_4$ selectivity and much higher CO_2/CH_4 selectivity, which indicates that this unique OH-functionalized PIM-PI membrane can be a very promising candidate for aggressive sour gas separations. Although PIM-6FDA-OH performance is similar to that of the crosslinked TEGMC and DEGMC, the avoidance of the need to crosslink the PIM-6FDA-OH may be a practical advantage.

Based on the mixed gas permeation results, the performance of thermally annealed PIM-6FDA-OH films for aggressive sour gas separations appears quite promising. However, due to the inherent differences between rubbery and glassy polymers in terms of CO_2/CH_4 and $\text{H}_2\text{S}/\text{CH}_4$ separations, it is difficult to compare the efficiency of these two different material types for the overall sour gas separation. Therefore, it is helpful to use a separation efficiency term referred to as “combined acid gas selectivity (α_{CAG})” that takes both of the separations into account, giving a measure of overall performance of different

Table 3 Comparison of PIM-6FDA-OH with other polymers in ternary mixed gas feeds at 35 °C

Polymer	Pressure (bar)	Feed composition (mol%) ($\text{H}_2\text{S}/\text{CO}_2/\text{CH}_4$)	Permeability (Barrer)		Selectivity		Reference
			CO_2	H_2S	CO_2/CH_4	$\text{H}_2\text{S}/\text{CH}_4$	
PIM-6FDA-OH	34.5	15/15/70	54.7	36.0	27.8	18.3	This work
PIM-6FDA-OH	48.3	15/15/70	52.6	63.0	25.0	30.0	This work
Cross-linked TEGMC	48.3	20/20/60	46.2	33.5	31.2	22.5	24
Cross-linked DEGMC	48.3	20/20/60	54.6	38.2	28.4	19.3	24
Cellulose acetate	34.5	20/20/60	8.66	8.71	29.5	29.7	4
Cellulose acetate	48.3	20/20/60	27.5	39.7	19.1	27.4	4
Cellulose acetate	10.1	6/29/65	2.43	2.13	22	19	11
6FDA-DAM : DABA (3 : 2) annealed 180 °C	48.3	10/20/70	55.6	25.4	32.1	14.7	22
6FDA-DAM : DABA (3 : 2) annealed 230 °C	48.3	10/20/70	50.8	23.6	31.1	14.4	22
Pebax 1074	10.1	12.5/18.1/69.4	155	695	11	50	11
PU1	10.1	12.5/18.1/69.4	55.8	183	6.9	23	11
PU2	10.1	12.5/18.1/69.4	195	618	5.6	18	11
PU3	10.1	12.5/18.1/69.4	62.2	280	12	55	11
PU4	10.1	12.5/18.1/69.4	50.8	223	15	66	11
6F-PAI-1	63.3	10/20/70	8.1	4.2	32	11	21



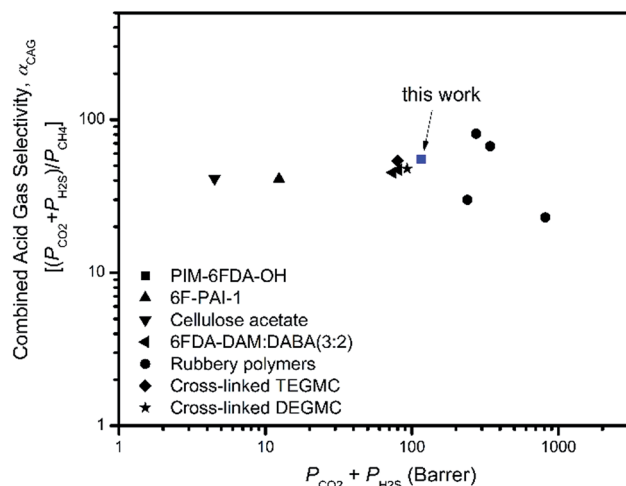


Fig. 14 Productivity-efficiency trade-off for combined acid gas separations. Ternary gas data are shown for rubbers (black symbols) as well as PIM-6FDA-OH and some other glassy polymers, 6F-PAI-1, CA and 6FDA-DAM : DABA (3 : 2). The data points for PIM-6FDA-OH, 6F-PAI-1, and 6FDA-DAM : DABA (3 : 2) correspond to ternary sour gas mixtures with a total feed pressure greater than 34.5 bar (15% H₂S, 15% CO₂, 70% CH₄ for PIM-6FDA-OH; 10% H₂S, 20% CO₂, 70% CH₄ for 6F-PAI-1 and 6FDA-DAM : DABA (3 : 2)); CA data were tested under 10.1 bar with ternary sour gas mixtures 6% H₂S, 29% CO₂, and 65% CH₄; rubbery polymers were tested under 10.1 bar with ternary sour gas mixtures 12% H₂S, 18% CO₂, and 70% CH₄; the data for 6F-PAI-1 are adapted from ref. 21; the data for 6FDA-DAM : DABA (3 : 2) are adapted from ref. 22; the data for CA and the rubbery polymers are adapted from ref. 11. The data for crosslinked PEGMC are adapted from ref. 24.

polymer materials. The so-called “combined acid gas selectivity (α_{CAG})” is defined as the ratio of combined acid gas permeability ($P_{\text{H}_2\text{S}} + P_{\text{CO}_2}$) and methane permeability (P_{CH_4}). Using this parameter, the results of this work are compared to the literature data in Table 3 through a combined acid gas productivity ($P_{\text{H}_2\text{S}} + P_{\text{CO}_2}$)-efficiency (α_{CAG}) trade-off plot (Fig. 14). It can be seen that the location of PIM-6FDA-OH near the upper right quadrant indicates that this material performs significantly better than CA and 6F-PAI based on the combined acid gas metric. It also appears to be very competitive with the majority of the rubbery polymers. Moreover, the sour gas testing conditions considered here are more aggressive than those examined with these rubbery materials. An additional factor to mention is the ultimate form which practical membranes will take for acid gas treatment. Specifically, asymmetric hollow fibers with very high surface to volume packing efficiency are desired. Both the glassy 6FDA-DAM-DABA and PIM-6FDA-OH have the practical ability to be formed into ultrathin selective layers ($\leq 0.1 \mu\text{m}$). On the other hand, forming defect-free rubbery selective layers less than one micron is very challenging. Furthermore, the $P/l = n_c/\Delta f_{\text{ci}}$, the true measure of productivity of the two glassy polymers may exceed that of corresponding rubbery materials such as those shown in Fig. 14. Formation of such high performance asymmetric glassy polymer membranes based on either 6FDA-DAM-DABA or PIM-6FDA-OH is beyond the scope of the current work. Nevertheless, addressing the relative ease of forming such

membranes will be important objectives in our work. Alternative PIM materials are currently explored in our groups to further improve the performance for aggressive sour gas separations.^{50–53}

Conclusions

A hydroxyl-functionalized polymer with intrinsic microporosity (PIM-6FDA-OH) was successfully synthesized using 3,3,3',3'-tetramethyl-1,1'-spirobisindane-5,5'-diamino-6,6'-diol with 6FDA. Aggressive sour gas separations using thermally annealed PIM-6FDA-OH films with pure and mixed gases were investigated through permeation and sorption testing. Pure gas permeation tests on the thermally annealed PIM-6FDA-OH films showed that this novel polymer is more permeable than most traditional polyimides owing to the intrinsic microporosity introduced by the OH-containing PIM segments. H₂S-induced plasticization did not occur until approximately 4.5 bar feed pressure, and CO₂-induced plasticization was not apparent until greater than 28 bar, indicating greatly improved CO₂ and H₂S plasticization resistance compared to unannealed films and other 6FDA-based polyimide materials. Mixed gas permeation results showed that at the highest test pressures, excellent CO₂/CH₄ selectivity was still maintained, while the H₂S/CH₄ selectivity reached nearly 30 in the thermally annealed PIM-6FDA-OH film. This selectivity is much better than that of most other glassy polymers and is very competitive even compared with rubbery polymers. Based on the pure and mixed gas transport results of this study, the novel PIM-6FDA-OH materials appear to provide excellent acid gas permeability, CO₂/CH₄ selectivity, H₂S/CH₄ selectivity, and much improved penetrant-induced plasticization resistance. By introducing the combined acid gas selectivity, the productivity and efficiency performance of glassy and rubbery polymer membranes for sour gas separations were compared, showing that the hydroxyl-functionalized PIM-PI polymer is potentially a very promising candidate for aggressive sour gas separations.

Acknowledgements

The authors would like to thank King Abdullah University of Science and Technology (KAUST) for generously funding this work (Award No. KUS-I1-011-21 for William Koros and KAUST CCF funding for Ingo Pinnau).

Notes and references

- 1 The U.S. Energy Information Administration (EIA), *Annual Energy Outlook 2014*, Release Date, May 7, 2014.
- 2 R. W. Baker and K. Lokhandwala, *Ind. Eng. Chem. Res.*, 2008, **47**, 2109–2121.
- 3 J. T. Vaughn, W. J. Koros, J. R. Johnson and O. Karvan, *J. Membr. Sci.*, 2012, **401–402**, 163–174.
- 4 C. S. K. Achoundong, N. Bhuwania, S. K. Burgess, O. Karvan, J. R. Johnson and W. J. Koros, *Macromolecules*, 2013, **46**, 5584–5594.



- 5 D. M. Amirkhanov, A. A. Kotenko, M. N. Tul'skii and M. M. Chelyak, *Fibre Chem.*, 2001, **33**, 67–72.
- 6 C. J. Orme and F. F. Stewart, *J. Membr. Sci.*, 2005, **253**, 243–249.
- 7 B. D. Bhide, A. Voskericyan and S. A. Stern, *J. Membr. Sci.*, 1998, **140**, 27–49.
- 8 W. Qiu, C. C. Chen, L. Xu, L. Cui, D. R. Paul and W. J. Koros, *Macromolecules*, 2011, **44**, 6046–6056.
- 9 Y. F. Li, Q. P. Xin, H. Wu, R. L. Guo, Z. Z. Tian, Y. Liu, S. F. Wang, G. W. He, F. S. Pan and Z. Y. Jiang, *Energy Environ. Sci.*, 2014, **7**, 1489–1499.
- 10 N. Y. Du, H. B. Park, M. M. Dal-Cin and M. D. Guiver, *Energy Environ. Sci.*, 2012, **5**, 7306–7322.
- 11 G. Chatterjee, A. A. Houde and S. A. Stern, *J. Membr. Sci.*, 1997, **135**, 99–106.
- 12 L. M. Robeson, *J. Membr. Sci.*, 2008, **320**, 390–400.
- 13 L. M. Robeson, *J. Membr. Sci.*, 1991, **62**, 165–185.
- 14 L. Xu, C. Zhang, M. Rungta, W. Qiu, J. Liu and W. J. Koros, *J. Membr. Sci.*, 2014, **459**, 223–232.
- 15 C. Ma and W. J. Koros, *J. Membr. Sci.*, 2013, **428**, 251–259.
- 16 Q. L. Song, S. K. Nataraj, M. V. Roussanova, J. C. Tan, D. J. Hughes, W. Li, P. Bourgoïn, M. A. Alam, A. K. Cheetham, S. A. Al-Muhtaseb and E. Sivaniah, *Energy Environ. Sci.*, 2012, **5**, 8359–8369.
- 17 L. Cui, W. Qiu, D. R. Paul and W. J. Koros, *Polymer*, 2011, **52**, 3374–3380.
- 18 I. C. Omole, S. J. Miller and W. J. Koros, *Macromolecules*, 2008, **41**, 6367–6375.
- 19 J. H. Kim, W. J. Koros and D. R. Paul, *Polymer*, 2006, **47**, 3094–3103.
- 20 M. R. Coleman and W. J. Koros, *J. Membr. Sci.*, 1990, **50**, 285–297.
- 21 J. T. Vaughn and W. J. Koros, *J. Membr. Sci.*, 2014, **465**, 107–116.
- 22 B. Kraftschik, W. J. Koros, J. R. Johnson and O. Karvan, *J. Membr. Sci.*, 2013, **428**, 608–619.
- 23 S. Keskin and D. S. Sholl, *Energy Environ. Sci.*, 2010, **3**, 343–351.
- 24 B. Kraftschik and W. J. Koros, *Macromolecules*, 2013, **46**, 6908–6921.
- 25 J. D. Wind, D. R. Paul and W. J. Koros, *J. Membr. Sci.*, 2004, **228**, 227–236.
- 26 J. D. Wind, S. M. Sirard, D. R. Paul, P. F. Green, K. P. Johnston and W. J. Koros, *Macromolecules*, 2003, **36**, 6433–6441.
- 27 A. M. Kratochvil and W. J. Koros, *Macromolecules*, 2010, **43**, 4679–4687.
- 28 J. R. Wiegand, Z. P. Smith, Q. Liu, C. T. Patterson, B. D. Freeman and R. L. Guo, *J. Mater. Chem. A*, 2014, **2**, 13309–13320.
- 29 L. M. Robeson, Z. P. Smith, B. D. Freeman and D. R. Paul, *J. Membr. Sci.*, 2014, **453**, 71–83.
- 30 T. Mohammadi, M. T. Moghadam, M. Saeidi and M. Mahdaryfar, *Ind. Eng. Chem. Res.*, 2008, **47**, 7361–7367.
- 31 W. J. Koros, D. R. Paul and A. A. Rocha, *J. Polym. Sci., Part B: Polym. Phys.*, 1976, **14**, 687–702.
- 32 W. J. Koros, A. H. Chan and D. R. Paul, *J. Membr. Sci.*, 1977, **2**, 165–190.
- 33 W. J. Koros, *J. Polym. Sci., Part B: Polym. Phys.*, 1980, **18**, 981–992.
- 34 W. J. Koros, R. T. Chern, V. Stannett and H. B. Hopfenberg, *J. Polym. Sci., Part B: Polym. Phys.*, 1981, **19**, 1513–1530.
- 35 X. Ma, R. Swaidan, Y. Belmabkhout, Y. Zhu, E. Litwiller, M. Jouiad, I. Pinnau and Y. Han, *Macromolecules*, 2012, **45**, 3841–3849.
- 36 A. L. Kohl and R. Nielsen, *Gas purification*, Gulf Professional Publishing, 1997.
- 37 R. Swaidan, B. Ghanem, E. Litwiller and I. Pinnau, *J. Membr. Sci.*, 2015, **475**, 571–581.
- 38 C. S. K. Achoundong, PhD dissertation, Georgia Institute of Technology, 2013.
- 39 T. T. Moore, S. Damle, P. J. Williams and W. J. Koros, *J. Membr. Sci.*, 2004, **245**, 227–231.
- 40 S. Damle and W. J. Koros, *Ind. Eng. Chem. Res.*, 2003, **42**, 6389–6395.
- 41 K. C. O'Brien, W. J. Koros, T. A. Barbari and E. S. Sanders, *J. Membr. Sci.*, 1986, **29**, 229–238.
- 42 L. M. Costello and W. J. Koros, *Ind. Eng. Chem. Res.*, 1992, **31**, 2708–2714.
- 43 C. H. Jung and Y. M. Lee, *Macromol. Res.*, 2008, **16**, 555–560.
- 44 P. M. Budd, K. J. Msayib, C. E. Tattershall, B. S. Ghanem, K. J. Reynolds, N. B. McKeown and D. Fritsch, *J. Membr. Sci.*, 2005, **251**, 263–269.
- 45 B. S. Ghanem, N. B. McKeown, P. M. Budd, J. D. Selbie and D. Fritsch, *Adv. Mater.*, 2008, **20**, 2766–2771.
- 46 W. J. Koros and D. R. Paul, *J. Polym. Sci., Part B: Polym. Phys.*, 1976, **14**, 1903–1907.
- 47 O. Esekhiile, W. L. Qiu and W. J. Koros, *J. Polym. Sci., Part B: Polym. Phys.*, 2011, **49**, 1605–1620.
- 48 M. Das and W. J. Koros, *J. Membr. Sci.*, 2010, **365**, 399–408.
- 49 H. D. Kamaruddin and W. J. Koros, *J. Membr. Sci.*, 1997, **135**, 147–159.
- 50 R. Swaidan, B. S. Ghanem, E. Litwiller and I. Pinnau, *J. Membr. Sci.*, 2014, **457**, 95–102.
- 51 R. Swaidan, M. Al-Saeedi, B. Ghanem, E. Litwiller and I. Pinnau, *Macromolecules*, 2014, **47**, 5104–5114.
- 52 B. S. Ghanem, R. Swaidan, X. Ma, E. Litwiller and I. Pinnau, *Adv. Mater.*, 2014, **26**, 6696–6700.
- 53 B. S. Ghanem, R. Swaidan, E. Litwiller and I. Pinnau, *Adv. Mater.*, 2014, **26**, 3688–3692.

